PAPER

Check for updates

Comparative study of antidiabetic, bactericidal, and antitumor activities of MEL@AgNPs, MEL@ZnONPs, and Ag–ZnO/MEL/GA nanocomposites prepared by using MEL and gum arabic

Abdelmoneim Bakur, [ID] [ab] Tarig Elshaarani,[c] Yongwu Niu[a] and Qihe Chen*[a]

In this study, a variety of nanocomposites, namely, MEL@AgNPs, MEL@ZnONPs, and Ag–ZnO/MEL/GA were biosynthesized using MEL and gum arabic to serve in biomedical applications. The synthesized nanocomposites were examined using X-ray diffraction (XRD), transmission electron microscopy (TEM), scanning electron microscopy (SEM), and FTIR spectroscopy. The physicochemical properties and biomedical activities of the synthesized nanocomposites were investigated. The Ag–ZnO/MEL/GA nanocomposites showed greater antidiabetic activity against α-amylase and α-glucosidase, and higher antibacterial activity compared to MEL@AgNPs and MEL@ZnONPs. Furthermore, HepG2 cells were exposed to MEL@AgNPs, MEL@ZnONPs, and Ag–ZnO/MEL/GA nanocomposites for 24 h and their IC_{50} values were 63.25, 26.91 and 28.97 $\mu g\ mL^{-1}$ ($P < 0.05$), respectively. According to this comparative study, it is apparent that the Ag–ZnO/MEL/GA nanocomposites have a great potential to serve as antitumor agents against HepG2, and antidiabetic and antibacterial agents.

1. Introduction

Recently, the number of infections of pathogenic bacteria has increased and become a major health concern. The resistance of bacteria to antibiotics, and the appearance of new bacterial mutations, as well as a lack of drugs in underdeveloped countries, raise the demand for an effective and eco-friendly bactericidal agent.[1,2] Resistance free bactericidal agents would be beneficial, particularly for foodborne diseases such as *Escherichia coli*, *Staphylococcus aureus*, *Pseudomonas aeruginosa*, *Salmonella types*, and *Clostridium perfringens*. Another major health concern is diabetes, which is a set of metabolic dysfunctions due to either defects in resistance or secretion of insulin. This disease causes the blood's glucose level to elevate; currently more than 387 million adults are affected in the worldwide.[3] Nowadays, diabetes treatment is extensively studied using nanomaterials. They are small, biocompatible and have a high drug loading capacity and efficiency.[4,5] Therefore, the development of new nanomedicine is increasingly required to inhibit carbohydrate-hydrolysing enzymes with minimum side effects.[6] Another disease that can be treated using nanocomposites is cancer, which is a multifunctional

disease which occurs when the proliferation of cells becomes uncontrolled. Cancer is one of the major causes of death throughout the world. Hepatocellular carcinoma (HCC) which is a kind of liver cancer has become one of the top four aggressive tumors around the globe.[7,8] Therefore, new treatment of these diseases is highly demanded.

Nanocomposites are materials that can be produced by incorporating two or more nano-fillers. In recent years they have attracted much attention due to their excellent multifunctional attributes and improved properties over a monometallic NPs.[9] In this regard, composites containing both noble metal NPs and metal oxide are more attractive and have great potential in the biomedical domains. Among them, ZnONPs have gained more attention due to its functional properties. The photocatalytic and antimicrobial activities of ZnONPs can be enhanced through doping with Ag to produce Ag–ZnO.[10] The interaction between ZnO and Ag in the Ag–ZnO composites provides an excellent inhibition of the bacterial growth.[11,12] The properties of nanocomposites depend on their size, shape, interfacial characteristics, as well as the nature of nano-fillers.[13,14] In line with this, biosurfactants have been emerged as an alternative green materials for the synthesis of NPs compared to the physiochemical and biological processes, biosurfactants are biodegradable, stable, less toxic, uniform in shape, and have improved biomedical activities of metallic NPs.[15–19]

In the current study, we used promising microbial surfactants, mannosylerythritol lipids (MEL), because of their various potential bioactivities, such as antimicrobial activity,

[a]*Department of Food Science and Nutrition, Zhejiang University, Hangzhou 310058, China. E-mail: chenqh@zju.edu.cn*

[b]*Department of Food Sciences and Technology, University of Kordofan, El Obeid 51111, Sudan*

[c]*College of Chemical and Biological Engineering, Zhejiang University, Hangzhou 310027, China*

antioxidant, interfacial, and antitumor properties. MEL has been used in many fields, *e.g.* pharmaceutical, environmental, and cosmetic.[20–24] MEL has also gained particular attention due to their behavior of self-assembling properties could be utilized in gene transfection and drug delivery.[25] As evident from previous reports, biosurfactants have ability to mediate the synthesis of NPs as both reducing and stabilizing agents, such as rhamnolipid, sophorolipids, and lipopeptide bio-surfactant.[18,26,27] Gum arabic (GA, E-414) is an edible and dried exudation obtained from the stems and branches of *Acacia senegal*. It is widely used as a thickening, emulsifier and stabilizer agent for food, pharmaceutical and cosmetics industries.[28] GA also has been extended to use in the nanomedicine domains, because of its biocompatible for *in vivo* applications and excellent stabilization of nanomaterials.[29]

In the last decade, many methods and techniques are developed to fabricate nanocomposites using biosurfactants or biopolymer ingredients to obtain a unique multifunctional. Notable examples include sol-cast transformation method, which was used to synthesize GC/PEG/ZnO/Ag nanocomposites films.[30] Also, the deposition–precipitation method was used to synthesize chitosan–Ag/ZnO nanocomposites.[31] Solution casting is another method of preparing nanocomposites. Ag-doped ZnO as nanofiller with cashew gum and chitin was prepared through this method.[32] Sol–gel technique was also used to prepare ZnONPs using *Pseudomonas aeruginosa* rhamnolipids.[33] Also, the electrospinning process was employed to produce Ag–ZnO bimetallic nanoencapsulated in PVP/PCL nanofibres.[34]

Here, we focused on developing a novel, facile, and eco-friendly nanocomposites consisting of Ag and ZnO NPs coated by biopolymers (gum arabic) and biosurfactants (MEL) to serve as antidiabetic, antitumor, and bactericidal agents. To best of our knowledge, there was no study available on the synthesis of ZnO and Ag NPs using the mannosylerythritol lipids (MEL).

2. Experimental details

2.1. Materials

Gum arabic (GA, from acacia tree), a mannosylerythritol lipid (MEL) was provided by fermentation engineering lab, Dep. of Food Science and Nutrition, Zhejiang University, China. Zinc acetate dehydrate $(Zn(CH_3COO)_2 \cdot 2H_2O)$, and silver nitrate $(AgNO_3)$ were purchased from Sinopharm Chemical Reagent Co., Ltd. China. All the other reagents were utilized as received at analytical reagent grade.

2.2. Synthesis of nanocomposites

2.2.1. Synthesis of MEL@AgNPs. The MEL was employed as both the reducing and stabilizing agents in bioreduction of silver ions. 200 μL of MEL in 1 mL of methanol diluted to 10 mL with DI water was mixed with an aqueous solution of 2 mM $AgNO_3$ in alkaline medium 0.1 M KOH under magnetic stirring at 80 °C for 30 min. Then, incubated overnight at 40 °C. The change of color to brown visually appeared the formation of AgNPs.

2.2.2. Synthesis of MEL@ZnONPs. ZnONPs were synthesized using zinc acetate dihydrate $(Zn(C_2H_3O_2)_2 \cdot 2H_2O)$ as a precursor. Typically, 1.2 g of zinc acetate was dissolved in 50 mL aqueous MEL solution under vigorous stirring until it becomes homogeneous. Then, few drops of 0.1 M KOH solution were added. The solution mixture was allowed to stir at 90 °C for 1 h. The whitish paste was washed 3 times with distilled water and ethanol and calcined at 500 °C for 2 h.

2.2.3. Synthesis of Ag–ZnO/MEL/GA nanocomposite. To prepare Ag–ZnO/MEL/GA nanocomposite, ZnO was incorporated into Ag and coated by MEL and GA. Briefly, AgNPs were dispersed in an aqueous solution of GA (50 mL, 1 mg mL^{-1}). The suspension was sonicated for 30 min using an ultrasonic bath sonicator. Then, 1 g of zinc acetate was dissolved in 50 mL aqueous MEL solution. The prepared solutions were thoroughly mixed with ratio 1 : 1 using magnetic stirring. After that, 0.1 M solution of KOH was added dropwise to the mixture under continuous stirring at ≥90 °C for 4 h. At last, the nano-composites was thoroughly washed with distilled water and ethanol, and calcined at 500 °C for 2 h.

2.3. Characterization of nanocomposites

FTIR spectra of the MEL@AgNPs, MEL@ZnONPs, and Ag–ZnO/MEL/GA nanocomposites were analyzed using FTIR spectro-photometer model (Vector 22, Bruker, Germany) in the range of 4000–500 cm^{-1}. The crystallinity of the prepared nano-composites was investigated *via* Siemens X-ray diffraction (XRD) analysis. Dried powder of nanocomposites was drop-coated onto glass slide, and the XRD pattern was recorded in a range of 20–80° at 2θ angle. The machine voltage was 45 keV, the current was 20 mA, and Cu-Kα radiation was used as an X-ray source. Furthermore, the structural features of the samples were investigated using transmission electron microscopy (TEM) (JEM-1230, JEOL, Akishima, Japan). The suspended samples were dropped into carbon-coated copper grids, and the excess samples were removed from the grid by using a cone of a blotting paper. The prepared thin film was reserved in a grid box sequentially. Moreover, the nanocomposites morphology was analyzed using scanning electron microscopic (SEM) (TM-1000, Hitachi, Japan). Thin films were prepared on a carbon-coated copper grid by dropping the samples onto the grid's surface, and the excess solution was removed using a blotting paper. Then, the films were dried under a mercury lamp for 5 min.

2.4. Antidiabetic activity

2.4.1. α-Amylase inhibitory activity. The α-amylase inhibition activity was investigated according to a modified method.[35] To prepare α-amylase assay mixtures, tubes containing MEL@AgNPs, MEL@ZnONPs and Ag–ZnO/MEL/GA nano-composites with different concentrations (20–100 μg mL^{-1}), sodium phosphate buffer (0.5 mL, 20 mM, pH 6.9) and α-amylase (1 U mL^{-1}) were pre-incubated at 37 °C for 15 min. Then, 250 μL starch solution (1%) was added as a substrate and the tubes kept at 37 °C for another 15 min. The reaction was ended by adding 1 mL of the DNS reagent (1% 3,5-

dinitrosalicylic acid and 12% sodium potassium tartrate in 0.4 M NaOH). The tubes were heated in a boiling water bath for 15 min and then cooled to 25 °C. The absorbance of the samples was recorded at 540 nm using acarbose as a positive control. The tube containing only the enzyme was considered as a control with 100% enzyme activity. The inhibitory activity was expressed as the percentage of inhibition.

2.4.2. α-Glucosidase inhibitory activity. The inhibition activity of α-glucosidase was investigated according to a modified method.[35] In brief, the α-glucosidase assay mixture comprised the nanocomposites at a concentration of 20 to 100 μg mL^{-1}, and 150 μL of 0.1% M sodium phosphate buffer (pH 6.9), α-glucosidase (1 U mL^{-1}), was pre-incubated at 37 °C for 15 min. Then, 50 μL of 2 mM p-nitrophenyl-α-ᴅ-glucopyranoside in sodium phosphate buffer was added to the mixture and incubated at 37 °C for 20 min. The reaction was terminated by adding 50 μL of 0.1 M sodium carbonate (Na$_2$CO$_3$). The absorbance was measured at 405 nm using acarbose as the positive control. The tube containing the enzyme without samples was considered as the control with 100% enzyme activity. The inhibitory activity was expressed as the percentage of inhibition.

2.5. Bactericidal efficacy test

2.5.1. Well-diffusion technique. The bactericidal efficacy of biosynthesized nanocomposites was tested against food-borne pathogenic bacteria, Gram-negative bacteria (E. coli and S. enteric) and Gram-positive bacteria (B. cereus and S. aureus) by the well-diffusion technique. In this technique, bacterial suspensions at a concentration of 10^5 CFU mL^{-1} were spread on Mueller–Hinton agar (MHA) plates. Three wells with 6 mm diameter were established in each of these plates using sterile borer. 50 μL of each sample was added onto each well at aseptic conditions. The tested plates were incubated at 37 ± 2 °C for 24 h, and the inhibition zone was measured.

2.5.2. Morphological observation of the bacterial cells. The effect of the biosynthesized nanocomposites on the morphological cells was observed using a scanning electron microscope (SEM).[36] In the current study, E. coli was selected as a model bacterium at a density of about 10^8 CFU mL^{-1}. E. coli treated with different samples (Ag, ZnO and GA/MEL/ZnO/Ag) and the untreated bacteria (control) were incubated at 37 °C for 4 h. After that, the bacterial cells were collected by centrifugation (12 000 rpm, 8 min), and rinsed twice with PBS. About 2.5% of glutaraldehyde solution was utilized for cells fixation and dehydrated serially with an ethanol solution of 30%, 50%, 70%, 85%, 90%, and 100% concentration. After dehydration, the bacterial cells were dried with a critical point dryer, fixed on SEM support, sputtered with gold coating and observed in SEM (SEM, Model SU-8010, Hitachi, Japan). Furthermore, the TEM analysis was used to explore the bactericidal mechanism of the nanocomposites on E. coli cells. Thus, the fixation and dehydration steps were performed similarly to SEM steps. Then, a sequence of pre-treatment processes for the TEM analysis described by ref. 37 with slight medications were done, and the cells were observed under TEM (JEM-1230, JEOL, Akishima, Japan).

2.6. Antitumor activity

The MTT assay was used to investigate the inhibition activity of the biosynthesized nanocomposites against HepG2 cells. HepG2 cells were obtained from Shanghai Cell Bank of China and maintained in a humidified incubator 5% CO$_2$ at 37 °C, in DMEM (Dulbecco's Modification Eagle Medium) supplemented with 10% fetal bovine serum (FBS) and 1% antibiotics solution (100 U per mL penicillin and 100 μg per mL streptomycin). The HepG2 cells were placed into 96-well plates at a density of 1.25 × 10^5 cells per well and incubated for 24 h. After incubation, the cells were treated with the MEL@AgNPs, MEL@ZnONPs, and Ag–ZnO/MEL/GA nanocomposites at different concentrations (5–80 μg mL^{-1}). The untreated cells were used as a control. The proliferation activity of the cells was determined by adding 5.0 mg per mL MTT reagent after 24 h of incubation. Finally, the absorbance was recorded at 570 nm in a microtitre plate reader (Thermo Electron Corp, Asheville, NC). The viability of HepG2 cells was expressed as a percentage of the control culture value, which was considered 100% viable.

2.7. Statistical analysis

Statistical analysis was conducted using SPSS (version 19, USA). The data were expressed as a standard deviation (mean ± SD). The statistical significance of differences between groups was assessed using one-way analysis of variance (ANOVA). A significant difference was considered at ($p < 0.05$).

3. Results and discussion

Bearing in mind the need for greener bioprocess and novel enhancers for the synthesis nanomaterials using the microbial method. The advantages of using MEL over the surfactants due to their biocompatibility, excellent surface activity, diverse biochemical functions, and its wide range of applications.[38] MEL can be utilized as a vehicle for the gene, and drug delivery is owing to their capability to form stable vesicles or nanostructures, which are employed as models for the cellular and molecular process. Also, the efficiency of gene transfection into mammalian cells has been increased considerably by the cationic liposome bearing MEL.[20] Additionally, gums are emerging as biodegradable substances, which have been used as delivery systems.[39] Based on this approach, we have prepared Ag, ZnO and Ag–ZnO nanocomposites by using biocompatible materials MEL and GA.

3.1. Characterization of nanocomposites

The crystalline structure of Ag, ZnO, and Ag–ZnO/MEL/GA nanocomposites was identified by X-ray diffraction technique (Fig. 1). The XRD analysis of MEL@AgNPs revealed four diffraction peaks at $2\theta = 37.9°$, 44.17°, 64.32° and 77.42° that associated to the (111), (200), (220) and (311) planes of the crystal lattice, respectively (Fig. 1a). Similar diffraction peaks were obtained by Sorbiun et al.[40] XRD diffraction peaks of this nanocomposite emphasized the face-centered cubic (fcc) and the crystalline structure of AgNPs fabricated by MEL. Further, the diffraction peaks of MEL@ZnONPs at $2\theta = 31.60°$, 34.46°,

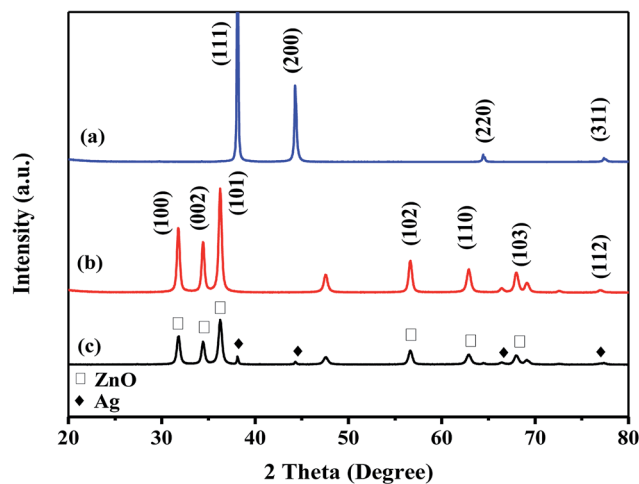Fig. 1 X-ray diffraction patterns of (a) MEL@AgNPs (b) MEL@ZnONPs (c) Ag−ZnO/MEL/GA nanocomposites.

Fig. 2 FTIR spectra of (a) MEL@ZnONPs (b) gum arabic (c) Ag−ZnO/MEL/GA nanocomposite (d) MEL@AgNPs (e) MEL.

$35.88°$, $47.46°$, $56.23°$, $62.74°$ and $68.03°$ were corresponded to (100), (002), (101), (102), (110), (103) and (112), respectively. These peaks confirmed the hexagonal wurtzite structure of ZnO (Fig. 1b). The results are consistent with the previously reported studies.[41] Eventually, Fig. 1c showed the XRD diffraction patterns of Ag−ZnO/MEL/GA nanocomposites. The diffraction peaks that designed with "◆" are attributed to AgNPs, while the diffraction peaks marked with "□" are related to the hexagonal wurtzite structure of ZnONPs. These diffraction peaks revealed that there is no notable shift in their position, and both the Ag and ZnO nanoparticles were successfully incorporated in the nanocomposites and attached to the surface of GA and MEL. The average crystallite size of Ag, ZnO and Ag−ZnO/MEL/GA nanocomposites was 43.14, 29.88, and 17.01 nm, respectively, obtained by the Scherrer formula.[33,42,43] Generally, the NPs obtained by MEL are almost similar to those obtained by other biosurfactants and slightly larger than those obtained by chemical surfactants.[17,44–46] The intensity of the diffraction peaks of ZnO in the nanocomposites became wider and weaker than that of pure ZnO. This was attributed to the decrement in the crystal size of ZnO when the ratio of Ag increased as the Ag could encapsulate ZnO and thus reduces the growth of ZnO crystal. A comparable phenomenon was stated in the earlier studies.[42,47]

The FTIR spectra were recorded to verify the possible interactions of MEL in MEL@AgNPs, MEL@ZnONPs and Ag−ZnO/MEL/GA nanocomposites. Fig. 2 exhibited stretching vibrations of MEL at 3374, 2945, 1453, and 724 cm^{-1} which are correspond to (O–H), (C–H), (C–H) and (C=O) absorption bands, respectively. These bands are consistent with other's work.[48] The absorption bands at 1453 and 2945 cm^{-1} confirmed the presence of the fatty acid chains. The bands of MEL in Ag and ZnO nanoparticles were shifting remarkably, which might be due to the reduction of Ag and ZnO.[49] GA displayed notable stretching vibration bands at 3386, 2920 and 1420 cm^{-1} that correspond to O–H stretching vibration of polymer, C–H stretching of CH_2 group and the deformations of the CH_2 group, respectively. These results are in a good agreement with other reports.[50–53] Finally,
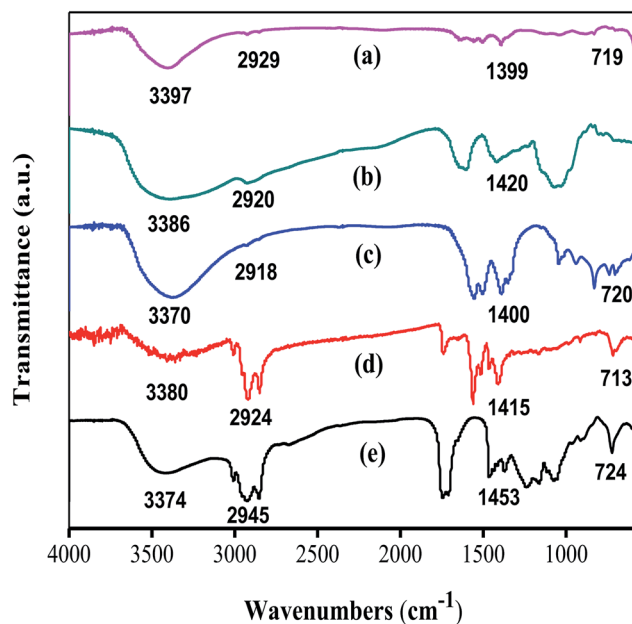
the absorption bands of Ag−ZnO/MEL/GA nanocomposites showed a minor shift and a low peak intensity compared to GA and MEL, which was ascribed to the strong intermolecular interactions between the functional groups in GA and MEL with Ag and ZnO NPs. Similar findings were also observed in the synthesized of ChNW/ZnO–Ag nanocomposites.[42]

Fig. 3a–c showed the SEM images of the morphology of MEL@AgNPs, MEL@ZnONPs, and Ag−ZnO/MEL/GA nanocomposites. SEM micrographs illustrated that both the Ag and ZnO NPs samples are spherical in shape, uniform and dispersed with small size.[40,54] Besides, the morphology of Ag−ZnO/MEL/GA nanocomposites exhibited a homogenous structure, smooth surface with slight agglomeration.[55,56] The Ag and ZnO NPs are uniformly distributed on the surface of GA and MEL. This could be due to the role of the mannosylerythritol lipids (MEL) on the morphology of the nanoparticles.

Additionally, the TEM images of MEL@AgNPs, MEL@ZnONPs, and Ag−ZnO/MEL/GA nanocomposites are shown in Fig. 3d–f. The images confirmed the spherical shape of nanocomposites. The average size the pure ZnO was 29.88 nm, while that of Ag−ZnO/MEL/GA nanocomposites was 17.01 nm. The small size of Ag−ZnO/MEL/GA nanocomposites was due to the increase in the Ag ratio.

3.2. Inhibition of α-amylase and α-glucosidase

Diabetes mellitus (DM) is multifunctional metabolic disorder characterized by inadequate secretion or weakened action of insulin resulting in high-level of blood sugar (hyperglycemia). The digestive enzymes (α-amylase and α-glucosidase) play an essential role in the digestion of carbohydrate.[57] In this study, the digestive enzymes α-amylase and α-glucosidase were used to assess the antidiabetic efficacy of the prepared MEL@AgNPs, MEL@ZnONPs, and Ag−ZnO/MEL/GA nanocomposites. As
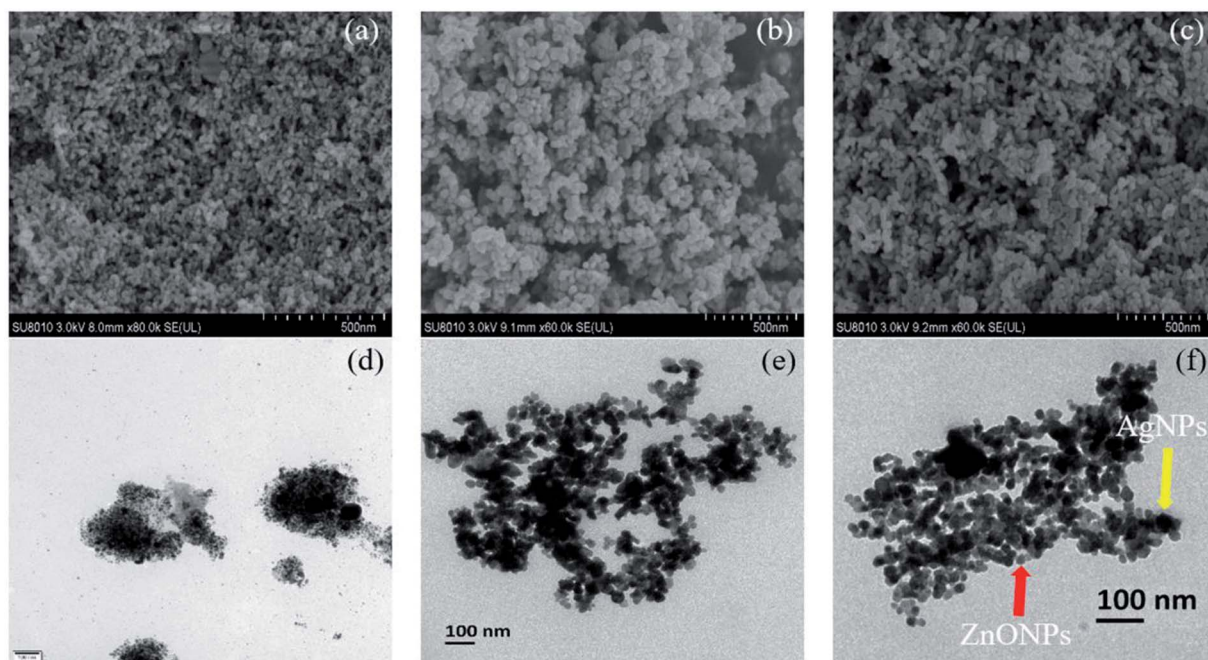
Fig. 3 SEM (a–c) and TEM (d–f) micrographs of MEL@AgNPs, MEL@ZnONPs, and Ag–ZnO/MEL/GA nanocomposite, respectively.

shown in Fig. 4, all three samples demonstrated significant inhibition in a concentration-dependent reduction for both digestive enzymes.

In the case of α-amylase inhibitory activity, Fig. 4a illustrates the IC_{50} values of Ag, ZnO, and Ag–ZnO/MEL/GA nanocomposites, which were found to be 54, 49, and 43 μg mL^{-1}, respectively. While in α-glucosidase inhibitory activity, these were found to be 51, 46, and 37, respectively (Fig. 4b). These results are consistent with other studies.[58–60] It has been found that the Ag–ZnO/MEL/GA nanocomposites show a potent antidiabetic activity in comparison with Ag and ZnO NPs, whereas ZnONPs revealed marginally higher activity compared with AgNPs in inhibition of α-amylase and α-glucosidase. Several publications have documented that the SPB1 biosurfactant could be a promising candidate for the treatment of diabetes in addition to delaying the later complications from it. The SPB1 biosurfactant has the ability to reduce the blood glucose level due to the efficiency of modulating the immune system leading to the decrease of β-cells damages. In diabetic group, lipid droplets were observed in the cytoplasm of hepatic and renal tissues, due to the lack of insulin responsible for metabolizing fats.[61] The chemical surfactants are usually used to enhance the solubility and delivery of antidiabetic drugs such as SDS, CTAB and Tween-80.[62] Also, Edwards and his colleagues[63] suggested that using different kind of gums could be effective in reducing postprandial hyperglycemia in human. Furthermore, zinc is one of the essential trace elements acting as insulin in the human body and enhances glucose consumption.[64,65] From the prior results, it can be concluded that the use of Ag–ZnO/MEL/GA nanocomposites, biosynthesized using the MEL and gum arabic, will be considerably helpful to inhibit the carbohydrate-digesting enzymes and could demonstrate an efficient way to control diabetes.

3.3. Bactericidal potential studies

3.3.1. Well-diffusion technique. The bactericidal activities of MEL@AgNPs, MEL@ZnONPs, and Ag–ZnO/MEL/GA nanocomposites were investigated against Gram-negative (*E. coli* and *S. enterica*) and Gram-positive (*B. cereus* and *S. aureus*) food pathogenic bacteria using the well-diffusion technique, and the results of the zone of inhibition (ZOI) are presented in Fig. 5. Generally, all these samples showed potential antibacterial efficacy against all pathogens. Besides, the statistically insignificant difference ($p > 0.05$) between the MEL@ZnONPs and MEL@AgNPs was found for all pathogenic bacteria, except for *E. coli* which were inhibited significantly by MEL@ZnONPs more than MEL@AgNPs (Fig. 5e). These findings are in good agreement with other works.[66] Interestingly, Ag–ZnO/MEL/GA nanocomposites exhibited a significantly higher efficacy compared to monometallic counterparts MEL@AgNPs and MEL@ZnONPs for all pathogenic food bacteria. This might be due to an incorporated effect of Ag and ZnO NPs with biomolecules existent in the MEL and GA, which enhance the antibacterial activity. Noteworthily, we observed that the Gram-negative bacteria (*E. coli* and *S. enterica*) were more resistant than Gram-positive (*B. cereus* and *S. aureus*) due to the external walls of Gram-negative bacteria, which is built mostly from tightly packed lipopolysaccharide leading to effectual resistibility barrier working as resistive against reactive oxygen species.[67,68] MEL has also demonstrated bactericidal activity particularly against Gram-positive bacteria. This may be attributed to the pattern of alkyl chain groups on the mannose moiety, which are important factors for bactericidal activity.[69] Also, the MIC of MEL against Gram-positive bacteria are significantly lower compared to those of Span 20, sucrose monolaurate and
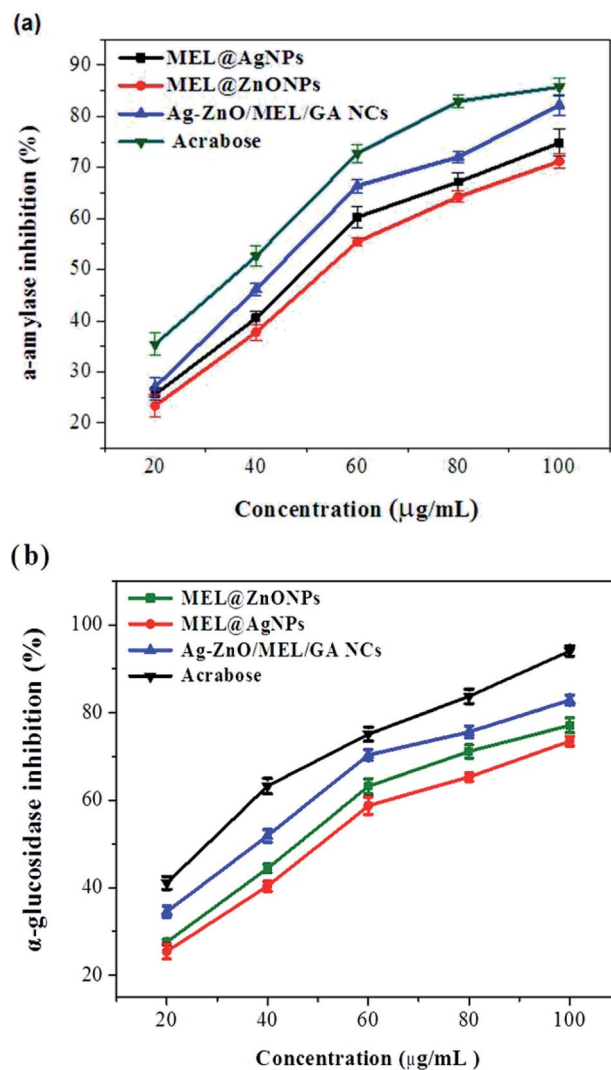
Fig. 4 Antidiabetic efficacy of the prepared MEL@AgNPs, MEL@ZnONPs and Ag–ZnO/MEL/GA nanocomposite based on inhibition of α-amylase and α-glucosidase.

sorbitan monoesters of fatty acids.[70] Silver based metallosurfactant prepared by using CTAB proved potent antimicrobial activity.[71] The inhibition of pathogenic bacteria by AgNPs,[58,72] ZnONPs[73,74] and Ag/ZnO nanocomposites[10,30,31] have been discussed in previous studies and operating of comparable mechanism is possible. Eventually, these findings suggest potential antimicrobial activities of Ag–ZnO/MEL/GA nanocomposites as a promising candidate for bactericidal drugs.

3.3.2. Study of the bactericidal action. TEM and SEM analysis of *E. coli* were used to explore the effect and action of the biosynthesized MEL@AgNPs, MEL@ZnONPs, and Ag–ZnO/MEL/GA nanocomposites on the bacterial cell. Fig. 6e and i shows that untreated cells seemed to be normal in shape with a smooth surface even the flagella can be seen; also the EDX analysis of the bacterial cells shows the absence of nanoparticles (Fig. 6a). In contrast, Fig. 6f and j shows that *E. coli* treated by MEL@AgNPs show the partially damaged walls and membranes (red arrows shows wall destroyed). Also, slight

morphological changes in lysed cells lead to cell death.[75] Fig. 6b confirmed the existence of Ag nanoparticles on the bacterial cells by EDX analysis. Fig. 6g and k shows that *E. coli* treated by MEL@ZnONPs displayed considerable cell-shrinkage or clumping and irregular structure (yellow arrows show cell-shrinkage). The presence of ZnO on the bacterial cells was verified by EDX analysis as shown in Fig. 6c. Meanwhile, *E. coli* treated with Ag–ZnO/MEL/GA nanocomposites showed severe cell-shrinkage and aggregation with broken walls and membranes (red and yellow arrows show cell-shrinkage and wall destroyed) as shown in Fig. 6h and l, which give rise to seepage of cell contents and consequently the death of bacteria. Further, the EDX analysis of the *E. coli*, treated by Ag–ZnO/MEL/GA nanocomposites, demonstrated the presence of elements of Ag and ZnO on the bacterial cell Fig. 6d. These results concur with other studies.[74–76] Potent antibacterial efficacy, with dual actions of the Ag–ZnO/MEL/GA nanocomposites against *E. coli* in comparison with Ag and ZnO nanoparticles, was observed.

Several mechanisms have been proposed for the antibacterial activity of silver NPs. For instance, silver NPs may adhere to the surface of the cell membrane disturbing permeability and respiration functions of the cell[17] but can also penetrate inside the bacteria.[77] Other hypothesis states that the deadly effect of Ag, resulting from the interaction of ionic silver with thiol groups, inhibits vital enzymes.[78,79] Moreover, other studies formulated hypothesis that ZnONPs can deform the wall and membrane of *E. coli* cells due to roughness and toxic oxygen radicals generated from the surface of ZnONPs, in addition, penetration of ZnO inside the cells of *E. coli* leads to membrane destroy, inhibition growth and finally cell death.[80,81] Furthermore, the gum arabic shows antibacterial activity against *E. coli* due to the phytochemical materials.[82] In addition to these, MEL has been demonstrated antimicrobial activity especially against Gram-positive bacteria.[83] Interestingly, other studies have verified the improved antibacterial actions of NPs synthesized by using surfactants, *e.g.*, Tween 80, CTAB, SDS, and polymers, *e.g.*, PVP 360.[16,84] So far, the exact mechanism behind the bactericidal activity is still not well known.

3.4. Cell viability assay

MTT assay was performed to evaluate the cytotoxicity effect of biosynthesized MEL@AgNPs, MEL@ZnONPs and Ag–ZnO/MEL/GA nanocomposites towards HepG2 cancer cells using increased concentration levels (5–80 μg mL^{-1}). Generally, the cell viability of HepG2 was decreased significantly with increasing the concentrations of the synthesized samples. The IC$_{50}$ values of biosynthesized MEL@AgNPs, MEL@ZnONPs and Ag–ZnO/MEL/GA nanocomposites for inhibition HepG2 cell were found to be 63.25, 26.91, and 28.97MG/ML, respectively (Fig. 7). It was observed that the HepG2 cells treated with the lower doses of 5 μg mL^{-1} do not show any significant cytotoxicity. Other researchers have reported similar results.[85] Interestingly, there was no significant difference between MEL@ZnONPs and Ag–ZnO/MEL/GA nanocomposites. In contrast, previous studies indicated that Ag–ZnO nanocomposites' cytotoxicity is lower than a MEL@ZnONPs in the
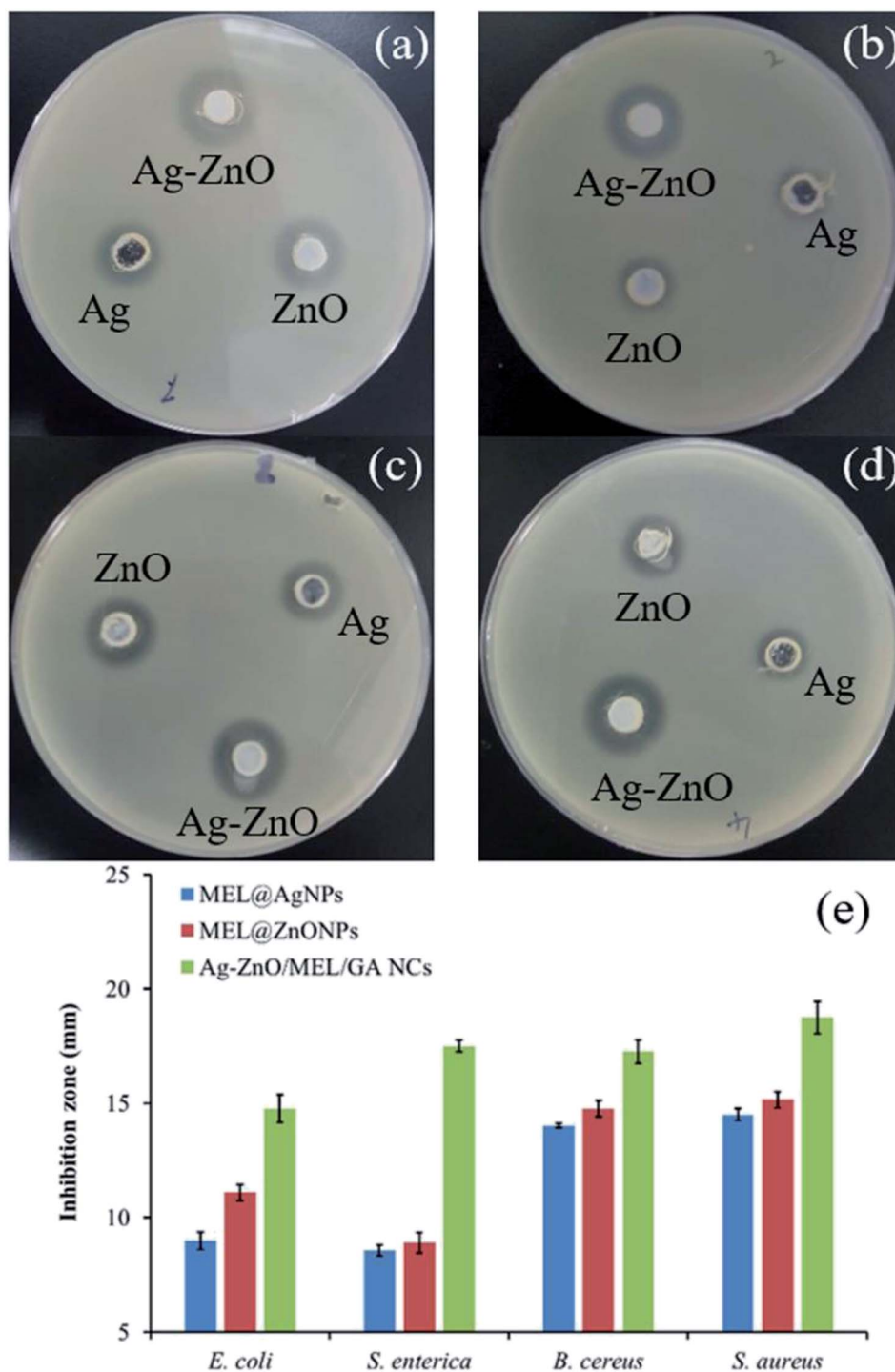
Fig. 5 Bactericidal efficacy of MEL@AgNPs, MEL@ZnONPs and Ag−ZnO/MEL/GA nanocomposite against (a) *E. coli* (b) *S. enterica* (c) *B. cereus* (d) *S. aureus* and (e) inhibitions zone of MEL@AgNPs, MEL@ZnONPs and Ag−ZnO/MEL/GA nanocomposites against bacteria. Different letters in each column refer significant differences ($P < 0.05$).

same dose range.[86] Arooj *et al.*[87] confirmed that the antitumor efficiency of Ag−ZnO NCs (with 10–30% Ag amount) were more than ZnONPs to malignant melanoma HT144 cells under daylight exposure. In our study, we did not determine the Ag content as well as did not use a light source to improve the cytotoxicity of Ag−ZnO NCs.

The reason for the potential antitumor activity of Ag−ZnO/MEL/GA nanocomposites might is due to the availability of biomolecules existing in both MEL and GA, which possessed antitumor efficacy against some cancer cells line. Besides the role of surfactants in NPs decoration, they play an important role in improving the solubility and cytotoxicity of anticancer
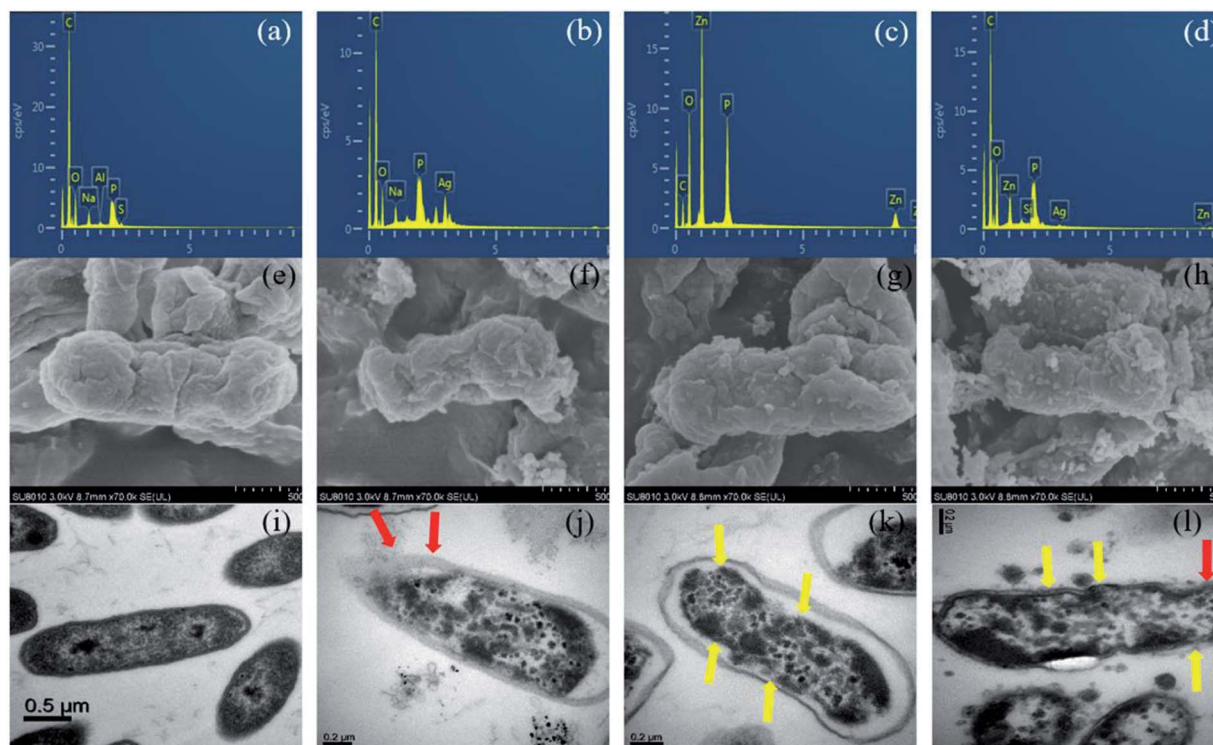
Fig. 6 EDX spectra (a−d), SEM (e−h) and TEM (i−l) analysis of untreated *E. coli*, treated with MEL@AgNPs, MEL@ZnONPs and Ag−ZnO/MEL/GA nanocomposites, respectively for each analysis.
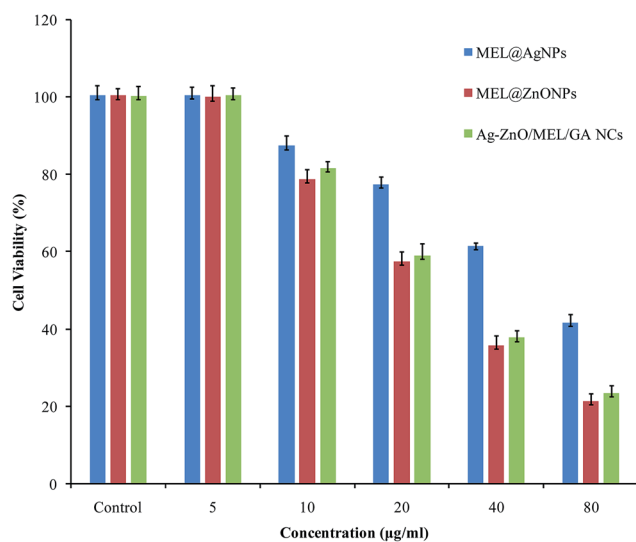

Fig. 7 Antitumor activity of various concentrations of MEL@AgNPs, MEL@ZnONPs and Ag−ZnO/MEL/GA nanocomposites against the liver cancer cell line HepG2.

drugs.[88] MEL has also induces tyrosinase activity and promotes the production of melanin.[23] Many studies reported the antitumor activity was enhanced with the presences of the surfactants.[71,88] Nevertheless, this is the first comparative study in the antitumor activity of Ag, ZnO and Ag−ZnO nanocomposites using MEL and GA against the HepG2 cell line. More studies are needed to figure out the biological mechanism of Ag−ZnO/MEL/GA nanocomposites.

4. Conclusions

In conclusion, we have successfully biosynthesized MEL@-AgNPs, MEL@ZnONPs and Ag−ZnO/MEL/GA nanocomposites using MEL and gum arabic. XRD, TEM, SEM, and FTIR spectroscopy confirmed the formation of these materials. Moreover, the biosynthesized materials demonstrated significant antidiabetic efficacy in a concentration-dependent reduction for the carbohydrate-digesting enzymes (α-amylase and α-glucosidase). The bactericidal efficacy was investigated against pathogenic food bacteria, Gram-negative (*E. coli* and *S. enterica*) and Gram-positive (*B. cereus* and *S. aureus*) using the well-diffusion technique, and the results of the zone of inhibition (ZOI) were measured. Also, the cytotoxicity test was performed against the human HepG2 cell line. However, further investigations are desired to explore the biological effects *in vivo* for the efficacy of Ag−ZnO/MEL/GA nanocomposites.

Conflicts of interest

There are no conflicts to declare.

Acknowledgements

References

1 K. L. Kotloff, J. P. Winickoff, B. Ivanoff, J. D. Clemens, D. L. Swerdlow, P. J. Sansonetti, G. K. Adak and M. M. Levine, *Bull. World Health Organ.*, 1999, **77**, 651–666.

2 Z.-C. Xiong, Z.-Y. Yang, Y.-J. Zhu, F.-F. Chen, Y.-G. Zhang and R.-L. Yang, *ACS Appl. Mater. Interfaces*, 2017, **9**, 22212–22222.

3 L. Guariguata, D. R. Whiting, I. Hambleton, J. Beagley, U. Linnenkamp and J. E. Shaw, *Diabetes Res. Clin. Pract.*, 2014, **103**, 137–149.

4 V. Karthick, V. G. Kumar, T. S. Dhas, G. Singaravelu, A. M. Sadiq and K. Govindaraju, *Colloids Surf., B*, 2014, **122**, 505–511.

5 R. Sharma, U. Gupta, N. K. Garg, R. K. Tyagi and N. K. Jain, *Colloids Surf., B*, 2015, **127**, 172–181.

6 U. Etxeberria, A. L. De La Garza, J. Campin, J. A. Martnez and F. I. Milagro, *Expert Opin. Ther. Targets*, 2012, **16**, 269–297.

7 D. S. Shewach and R. D. Kuchta, *Chem. Rev.*, 2009, **109**, 2859–2861.

8 Q. H. Ye, L. X. Qin, M. Forgues, P. He, J. W. Kim, A. C. Peng, R. Simon, Y. Li, A. I. Robles, Y. Chen, Z. C. Ma, Z. Q. Wu, S. L. Ye, Y. K. Liu, Z. Y. Tang and X. W. Wang, *Nat. Med.*, 2003, **9**, 416–423.

9 R. Sahay, V. J. Reddy and S. Ramakrishna, *Int. J. Mech. Mater. Eng.*, 2014, **9**, 25.

10 R. Aladpoosh and M. Montazer, *Carbohydr. Polym.*, 2016, **141**, 116–125.

11 S. Agnihotri, G. Bajaj, S. Mukherji and S. Mukherji, *Nanoscale*, 2015, **7**, 7415–7429.

12 I. Matai, A. Sachdev, P. Dubey, S. Uday Kumar, B. Bhushan and P. Gopinath, *Colloids Surf., B*, 2014, **115**, 359–367.

13 X. Xu, F. Liu, L. Jiang, J. Y. Zhu, D. Haagenson and D. P. Wiesenborn, *ACS Appl. Mater. Interfaces*, 2013, **5**, 2999–3009.

14 L. Zhang, J. Gu, L. Song, L. Chen, Y. Huang, J. Zhang and T. Chen, *J. Mater. Chem. A*, 2016, **4**, 10810–10815.

15 G. S. Kiran, J. Selvin, A. Manilal and S. Sujith, *Crit. Rev. Biotechnol.*, 2011, **31**, 354–364.

16 A. M. Alkilany, P. K. Nagaria, C. R. Hexel, T. J. Shaw, C. J. Murphy and M. D. Wyatt, *Small*, 2009, **5**, 701–708.

17 L. Kvítek, A. Panáček, J. Soukupová, M. Kolář, R. Večeřová, R. Prucek, M. Holecová and R. Zbořil, *J. Phys. Chem. C*, 2008, **112**, 5825–5834.

18 A. S. Reddy, C.-Y. Chen, S. C. Baker, C.-C. Chen, J.-S. Jean, C.-W. Fan, H.-R. Chen and J.-C. Wang, *Mater. Lett.*, 2009, **63**, 1227–1230.

19 Y. Xie, R. Ye and H. Liu, *Colloids Surf., A*, 2006, **279**, 175–178.

20 D. Kitamoto, T. Morita, T. Fukuoka, M.-a. Konishi and T. Imura, *Curr. Opin. Colloid Interface Sci.*, 2009, **14**, 315–328.

21 L. Fan, H. Li, Y. Niu and Q. Chen, *PLoS One*, 2016, **11**, e0148198.

22 Y. Wakamatsu, X. Zhao, C. Jin, N. Day, M. Shibahara, N. Nomura, T. Nakahara, T. Murata and K. K. Yokoyama, *Eur. J. Biochem.*, 2001, **268**, 374–383.

23 X. Zhao, Y. Wakamatsu, M. Shibahara, N. Nomura, C. Geltinger, T. Nakahara, T. Murata and K. K. Yokoyama, *Cancer Res.*, 1999, **59**, 482–486.

24 M. Takahashi, T. Morita, T. Fukuoka, T. Imura and D. Kitamoto, *J. Oleo Sci.*, 2012, **61**, 457–464.

25 Y. Inoh, D. Kitamoto, N. Hirashima and M. Nakanishi, *J. Controlled Release*, 2004, **94**, 423–431.

26 M. B. Kasture, P. Patel, A. A. Prabhune, C. V. Ramana, A. A. Kulkarni and B. L. V. Prasad, *J. Chem. Sci.*, 2008, **120**, 515–520.

27 E. Priyadarshini, N. Pradhan, A. K. Pradhan and P. Pradhan, *Spectrochim. Acta, Part A*, 2016, **163**, 127–133.

28 B. H. Ali, A. Ziada and G. Blunden, *Food Chem. Toxicol.*, 2009, **47**, 1–8.

29 A. C. A. Roque, A. Bicho, I. L. Batalha, A. S. Cardoso and A. Hussain, *J. Biotechnol.*, 2009, **144**, 313–320.

30 Y. Liu and H.-I. Kim, *Carbohydr. Polym.*, 2012, **89**, 111–116.

31 Z. Lu, J. Gao, Q. He, J. Wu, D. Liang, H. Yang and R. Chen, *Carbohydr. Polym.*, 2017, **156**, 460–469.

32 M. T. Ramesan, C. Siji, G. Kalaprasad, B. K. Bahuleyan and M. A. Al-Maghrabi, *J. Polym. Environ.*, 2018, **26**, 2983–2991.

33 B. N. Singh, A. K. S. Rawat, W. Khan, A. H. Naqvi and B. R. Singh, *PLoS One*, 2014, **9**, e106937.

34 M. Hu, C. Li, X. Li, M. Zhou, J. Sun, F. Sheng, S. Shi and L. Lu, *Artif. Cells, Nanomed., Biotechnol.*, 2018, **46**, 1248–1257.

35 K. Balan, W. Qing, Y. Wang, X. Liu, T. Palvannan, Y. Wang, F. Ma and Y. Zhang, *RSC Adv.*, 2016, **6**, 40162–40168.

36 Y. Zi, M. Zhu, X. Li, Y. Xu, H. Wei, D. Li and C. Mu, *Carbohydr. Polym.*, 2018, **192**, 118–125.

37 J. Yang, H. Lu, M. Li, J. Liu, S. Zhang, L. Xiong and Q. Sun, *Carbohydr. Polym.*, 2017, **178**, 311–321.

38 J. I. Arutchelvi, S. Bhaduri, P. V. Uppara and M. Doble, *J. Ind. Microbiol. Biotechnol.*, 2008, **35**, 1559–1570.

39 A. J. Ribeiro, F. R. L. de Souza, J. M. N. A. Bezerra, C. Oliveira, D. Nadvorny, M. F. de La Roca Soares, L. C. C. Nunes, E. C. Silva-Filho, F. Veiga and J. L. Soares Sobrinho, *Carbohydr. Polym.*, 2016, **147**, 188–200.

40 M. Sorbiun, E. Shayegan Mehr, A. Ramazani and S. Taghavi Fardood, *J. Mater. Sci.: Mater. Electron.*, 2018, **29**, 2806–2814.

41 S. B. Rana, V. K. Bhardwaj, S. Singh, A. Singh and N. Kaur, *J. Exp. Nanosci.*, 2014, **9**, 877–891.

42 A. A. Oun and J.-W. Rhim, *Carbohydr. Polym.*, 2017, **169**, 467–479.

43 S. Azizi, M. B. Ahmad, M. Z. Hussein and N. A. Ibrahim, *Molecules*, 2013, **18**, 6269–6280.

44 X. Lu, A. Dandapat, Y. Huang, L. Zhang, Y. Rong, L. Dai, Y. Sasson, J. Zhang and T. Chen, *RSC Adv.*, 2016, **6**, 60916–60921.

45 X. Lu, Y. Huang, B. Liu, L. Zhang, L. Song, J. Zhang, A. Zhang and T. Chen, *Chem. Mater.*, 2018, **30**, 1989–1997.

46 Y. Huang, L. Dai, L. Song, L. Zhang, Y. Rong, J. Zhang, Z. Nie and T. Chen, *ACS Appl. Mater. Interfaces*, 2016, **8**, 27949–27955.

47 S. Azizi, R. Mohamad, R. A. Rahim, A. B. Moghaddam, M. Moniri, A. Ariff, W. Z. Saad and F. Namvab, *Appl. Surf. Sci.*, 2016, **384**, 517–524.

48 T. Fukuoka, T. Morita, M. Konishi, T. Imura and D. Kitamoto, *J. Oleo Sci.*, 2007, **56**, 435–442.

49 S. Gomez-Grana, M. Perez-Ameneiro, X. Vecino, I. Pastoriza-Santos, J. Perez-Juste, J. M. Cruz and A. B. Moldes, *Nanomaterials*, 2017, **7**(6), 139.

50 M. M. Solomon, H. Gerengi, S. A. Umoren, N. B. Essien, U. B. Essien and E. Kaya, *Carbohydr. Polym.*, 2018, **181**, 43–55.

51 S. I. Alhassan, P. A. P. Mamza, A. M. Ja'o and D. E. Arthur, *SDRP Journal of Computational Chemistry & Molecular Modelling*, 2015, **1**, 1–8.

52 H. Adam, M. A. Siddig, A. A. Siddig and N. A. Eltahir, *Sudan Med. Monit.*, 2013, **8**, 174.

53 D. Mudgil, S. Barak and B. S. Khatkar, *Int. J. Biol. Macromol.*, 2012, **50**, 1035–1039.

54 L. Dai, L. Song, Y. Huang, L. Zhang, X. Lu, J. Zhang and T. Chen, *Langmuir*, 2017, **33**, 5378–5384.

55 Y. Huang, A. Dandapat and D.-H. Kim, *Nanoscale*, 2014, **6**, 6478–6481.

56 Y. Huang and D.-H. Kim, *Nanoscale*, 2012, **4**, 6312–6317.

57 V. Malapermal, I. Botha, S. B. N. Krishna and J. N. Mbatha, *Saudi J. Biol. Sci.*, 2017, **24**, 1294–1305.

58 G. D. Saratale, R. G. Saratale, G. Benelli, G. Kumar, A. Pugazhendhi, D.-S. Kim and H.-S. Shin, *J. Cluster Sci.*, 2017, **28**, 1709–1727.

59 D. Rehana, D. Mahendiran, R. S. Kumar and A. K. Rahiman, *Bioprocess Biosyst. Eng.*, 2017, **40**, 943–957.

60 A. Bayrami, S. Parvinroo, A. Habibi-Yangjeh and S. Rahim Pouran, *Artif. Cells, Nanomed., Biotechnol.*, 2018, **46**, 730–739.

61 R. Zouari, R. B. Abdallah-Kolsi, K. Hamden, A. E. Feki, K. Chaabouni, F. Makni-Ayadi, F. Sallemi, S. Ellouze-Chaabouni and D. Ghribi-Aydi, *Pept. Sci.*, 2015, **104**, 764–774.

62 N. Seedher and M. Kanojia, *AAPS PharmSciTech*, 2008, **9**, 431–436.

63 C. A. Edwards, N. A. Blackburn, L. Craigen, P. Davison, J. Tomlin, K. Sugden, I. T. Johnson and N. W. Read, *Am. J. Clin. Nutr.*, 1987, **46**, 72–77.

64 H. Haase, S. Overbeck and L. Rink, *Exp. Gerontol.*, 2008, **43**, 394–408.

65 J. Jansen, W. Karges and L. Rink, *J. Nutr. Biochem.*, 2009, **20**, 399–417.

66 W. Salem, D. R. Leitner, F. G. Zingl, G. Schratter, R. Prassl, W. Goessler, J. Reidl and S. Schild, *Int. J. Med. Microbiol.*, 2015, **305**, 85–95.

67 N. Papo and Y. Shai, *J. Biol. Chem.*, 2005, **280**, 10378–10387.

68 K. Y. Yoon, J. H. Byeon, C. W. Park and J. Hwang, *Environ. Sci. Technol.*, 2008, **42**, 1251–1255.

69 J. Nashida, N. Nishi, Y. Takahashi, C. Hayashi, M. Igarashi, D. Takahashi and K. Toshima, *J. Org. Chem.*, 2018, **83**, 7281–7289.

70 D. Kitamoto, H. Isoda and T. Nakahara, *J. Biosci. Bioeng.*, 2002, **94**, 187–201.

71 G. Kaur, S. Kumar, R. Kant, G. Bhanjana, N. Dilbaghi, S. K. Guru, S. Bhushan and S. Jaglan, *RSC Adv.*, 2016, **6**, 57084–57097.

72 V. K. Sharma, R. A. Yngard and Y. Lin, *Adv. Colloid Interface Sci.*, 2009, **145**, 83–96.

73 S. K. Basha, K. V. Lakshmi and V. S. Kumari, *Sens Biosensing Res.*, 2016, **10**, 34–40.

74 M. Arakha, M. Saleem, B. C. Mallick and S. Jha, *Sci. Rep.*, 2015, **5**, 9578.

75 Y.-H. Hsueh, K.-S. Lin, W.-J. Ke, C.-T. Hsieh, C.-L. Chiang, D.-Y. Tzou and S.-T. Liu, *PLoS One*, 2015, **10**, e0144306.

76 A. A. Tayel, W. F. El-Tras, S. Moussa, A. F. El-Baz, H. Mahrous, M. F. Salem and L. Brimer, *J. Food Saf.*, 2011, **31**, 211–218.

77 M. Jose Ruben, E. Jose Luis, C. Alejandra, H. Katherine, B. K. Juan, R. Jose Tapia and Y. Miguel Jose, *Nanotechnology*, 2005, **16**, 2346.

78 Y. Matsumura, K. Yoshikata, S. Kunisaki and T. Tsuchido, *Appl. Environ. Microbiol.*, 2003, **69**, 4278–4281.

79 A. Gupta, M. Maynes and S. Silver, *Appl. Environ. Microbiol.*, 1998, **64**, 5042–5045.

80 G. Applerot, A. Lipovsky, R. Dror, N. Perkas, Y. Nitzan, R. Lubart and A. Gedanken, *Adv. Funct. Mater.*, 2009, **19**, 842–852.

81 R. Brayner, R. Ferrari-Iliou, N. Brivois, S. Djediat, M. F. Benedetti and F. Fievet, *Nano Lett.*, 2006, **6**, 866–870.

82 S. M. A. Alawi, M. A. Hossain and A. A. Abusham, *Beni-Suef University Journal of Basic and Applied Sciences*, 2018, **7**, 22–26.

83 D. Kitamoto, H. Yanagishita, T. Shinbo, T. Nakane, C. Kamisawa and T. Nakahara, *J. Biotechnol.*, 1993, **29**, 91–96.

84 L. Kvitek, A. Panáček, J. Soukupova, M. Kolář, R. Večeřová, R. Prucek, M. Holecova and R. Zbořil, *J. Phys. Chem. C*, 2008, **112**, 5825–5834.

85 R. Wahab, M. A. Siddiqui, Q. Saquib, S. Dwivedi, J. Ahmad, J. Musarrat, A. A. Al-Khedhairy and H.-S. Shin, *Colloids Surf., B*, 2014, **117**, 267–276.

86 M. M. Rad, N. Najafzadeh, N. Tata and A. Jafari, *Pharmaceut. Chem. J.*, 2018, **52**, 112–116.

87 S. Arooj, S. Nazir, A. Nadhman, N. Ahmad, B. Muhammad, I. Ahmad, K. Mazhar and R. Abbasi, *Beilstein J. Nanotechnol.*, 2015, **6**, 570–582.

88 A. M. Alkilany and C. J. Murphy, *Langmuir*, 2009, **25**, 13874–13879.